AN EXPERIMENTAL INVESTIGATION ON THE SURFACE DEFORMATION OF A SOFT HALF PLANE INDENTED BY A RIGID WEDGE

Journal:	*Applied Mathematics and Mechanics (English Edition)*
Manuscript ID	AMM-2016-0212.R2
Manuscript Type:	Original Article
Date Submitted by the Author:	n/a
Complete List of Authors:	Tan, Xiaohua; Tianjin University of Technology and Education, Tianjin Key Lab of High Speed Cutting and Precision Machining; University of Liverpool Kang, Yilan; Tianjin University, Tianjin Key Laboratory of Modern Engineering Mechanics Patterson, Eann; The University of Liverpool, School of Engineering
Keywords:	Contact Mechanics, Wedge indentation, large deformation, Sector division, Digital image correlation
Speciality:	contact mechanics < Solids and fluid mechanics, interface mechanics < Solids and fluid mechanics

AN EXPERIMENTAL INVESTIGATION ON THE SURFACE DEFORMATION OF A SOFT HALF PLANE INDENTED BY A RIGID WEDGE

Xiaohua Tan[a,b], Yilan Kang[c] and Eann Patterson[b1]

a. Tianjin Key Lab of High Speed Cutting and Precision Machining, Tianjin University of Technology and Education, Tianjin, China, 300222

b. School of Engineering, University of Liverpool, United Kingdom, L69 3GH

c. Tianjin Key Laboratory of Modern Engineering Mechanics, School of Mechanical Engineering, Tianjin University, China, 300072

ABSTRACT: In this work, the mechanical behaviour of a block of soft material subject to large deformation from a series of wedge-shaped indenters has been evaluated. Data fields acquired from digital image correlation have been compared to existing theoretical models. The slope angles of the wedges varied from 5 to 73.5 degrees and the minimum measurement uncertainties of the digital image correlation system were established in advance to define the accuracy. It is concluded that the assumptions underpinning the analytical theory make it difficult to characterize large deformation of soft material during contact. The strain fields were also obtained from the measured displacement field and verified the previously postulated existence of two deformation sectors, namely, a so-called shrinkage sector symmetric to the loading axis and an expansion sector, which became smaller with increasing of load and decreasing wedge angle.

Key Words: Contact Mechanics; Wedge Indentation; Large Deformation; Sector Division; Digital Image Correlation

Mathematical Subject Classification: 74G99

[1] Corresponding author. Tel.: +44 151 794 4665; E-mail address: eann.patterson@liverpool.ac.uk

1. INTRODUCTION

Soft materials are used in important components in a wide range of products such as flexible electronics, surgical robots, and vibration absorbers. The nature of contact between the soft material and a rigid object is very important for many of these engineering applications. However, these materials present challenges to both the prediction and measurement of strain fields due the large deformation that they exhibit under relatively modest levels of applied load.

A rigid indenter pushed into an elastic body is representative of a number of engineering applications and has attracted the attention of many researchers. The classic paper of Boussinesq [1] first considered the distribution of stress within an elastic half space indented by a rigid punch. Based on this solution, Sneddon [2] derived some simple expressions for the distribution of pressure for several punch shapes. Subsequently, there have been several studies, e.g. [3, 4], concerned with the subsurface deformation of material produced by the indentation of wedges. Korsunsky [5] has shown that small variations in punch geometry have a significant influence on the contact strains. Gao and co-workers [6 - 8] have explored the behaviour of soft materials indented by rigid indenters from a theoretical perspective and suggested a 'sector division method' in which the strain field in the soft material block is partitioned into shrinking (SH) and expanding (EX) sectors that can be modelled separately.

It is worth mentioning, although the aforementioned theoretical models can provide solutions for some specific engineering problems, the validity of these models tends to be limited because most of the following assumptions are usually adopted: small elastic strains; the absence of shear tractions, i.e. the contact is frictionless; the contact zones are much smaller than the characteristic dimension of the bodies; similar elastic properties for the contacting bodies; and a small wedge angle. There is still a sparsity of experimental data describing the full-field deformation of soft elastic material during indentation by a rigid wedge and an experimental observation of the sector division concept is also lacking. Thus, the principal aim of this work was to provide more detailed data from experiments for use in evaluating and developing theoretical models. This has been achieved by extending the prior work that used a single wedge geometry [9]. Specifically, the measured data fields have been used

confirm the existence and evolution of the sectors identified by Gao & Gao [6] and to define the limits of applicability of the small deformation theory proposed by Ciavarella et al. [10].

2. EXPERIMENTAL APPARATUS AND PROCEDURE

The experimental arrangement used in this study was the same as used by Tan et al. [9], shown schematically in figure 1(a). Stereoscopic Digital Image Correlation (DIC) was employed for this work since traditional methods, such as strain gauges are not suitable for measuring large deformation over a large field of view [11]. DIC has many advantages such as being non-contact, high precision, real-time, and having a wide measurement range and a simple optical setup [12, 13]. In brief, a rectangular block of silicone rubber with dimensions 60mm×60mm×30mm was indented by an aluminium wedge of thickness 30mm with a tip radius of 1.68mm. Four wedges were used with slope angles of 5, 15, 45 and 73.5 degrees as shown in figure 1(b)~(e). One of the square surfaces of the rubber block was sprayed with an extremely thin layer of white paint (Matt Super White 1107, Plasti-kote, UK) on top of which was sprayed an even finer dusting of black paint (Matt Super Black 1102, Plasti-kote, UK) to form a speckle pattern, which was used to perform stereoscopic digital image correlation. A commercial DIC system (Q-400, Dantec Dynamics GmbH, Germany), was employed that had two cameras (FireWire, 1/8", 1624×1234 pixels) with 50mm focal length lenses resulting in a 35 pixels/mm magnification. The wedge was driven into the block at a constant speed of 1 mm/min while the specimen was illuminated with two green LED lights and pairs of images were captured at 30 seconds intervals.

The elastic modulus of the wedge and block were, according to the manufacturer's data, 73GPa and 2MPa respectively providing a large elastic dissimilarity and the contact surfaces were dry, i.e. there was no lubricant introduced. Difficulties are often occur when the DIC method is applied to large deformation measurements because of serious de-correlation between the reference image and the deformed image; hence a mixed Eulerian-Lagrangian approach was used in the digital image correlation, in which the reference images were updated when the level of deformation was sufficient to cause a loss of correlation. This approach is computational more efficient than updating the reference image at each increment and reduces the potential errors introduced during updating. The

sub-image or facet size for the correlation process was 25 pixels (≡ 0.7mm) and the facets were overlapped by 22 pixels to give displacement vectors at a pitch of 3 pixels or 0.084mm. A typical example of the surface displacement fields for the 15° wedge with a nominal indentation depth of 3.3mm (≡19.1 N) is shown in figure 2 with rigid body motions removed using the algorithm provided in the system software. The block always returned to its undeformed shape after indentation, i.e. all of the loading was elastic and there was no evidence of any adhesion between the indenter and block.

The uncertainty in the DIC measurements made using the set-up described above were previously assessed [9] using a protocol developed specifically for the purpose [14] and found to be 31.7με in-plane and 0.65μm out-of-plane.

3. EXPERIMENTAL RESULTS

3.1 Displacement fields

The measured surface displacement fields were compared with the predicted displacement fields from the solution due to Ciavarella et al. [10]. According to this solution for the half plane, the interior stress field is given by the following relations:

$$\begin{aligned} \sigma_x+\sigma_y &= 4\mathrm{Re}\Phi(z) \\ \sigma_y-\sigma_x+2i\tau_{xy} &= 2\left[(\bar{z}-z)\Phi'(z)-\overline{\Phi}(z)-\Phi(z)\right] \end{aligned} \tag{1}$$

where $z=x+iy$ is the complex form of the coordinates x and y which are defined as shown in figure 1 with the origin at the centre of contact. The corresponding Muskhelishvili's potential is

$$\Phi(z)=\frac{1}{2\pi i}\int_{contact}\frac{p(t)}{t-z}dt=\frac{1}{2i}\sum_{n=0}^{\infty}b_n[z-(z^2-1)^{1/2}]^{2n+1} \tag{2}$$

where $p(t)$ is the pressure distributed on the contact boundary.

In this work, the theoretical stress state in the region of interest was obtained by a numerical solution of equations (1) and (2). Following the assumptions made by Ciavarella et al. [10], there are two viable options for computing the interior displacement fields; they can be either deduced directly from the Muskhelishvili potential, or integrated from the corresponding strains that are converted from the stress state using Hooke's law [15]. It was found that the computation method has little effect on the final results and so the second option was used because it was computationally more

convenient. A quantitative comparison was made between the displacement fields measured in the experiments and those obtained from the theory. In this process, each field of displacement was treated as an image and decomposed using Tchebichef kernels [16] by a specially-written MATLAB® program. This process yielded a set of mathematical moments, which were a unique representation of the displacement field. The accuracy of the representation was checked by reconstructing the data fields from the Tchebichef moments. A 99% correlation between the original and reconstructed data fields was obtained by employing the first fifty Tchebichef moments and this was believed to be sufficient [16, 17]. This decomposition process was invariant to translation, scale and rotation while at the same time it decreased the dimensionality of the data and hence is a powerful tool for making quantitative comparisons [17], especially when the data fields do not share a coordinate system or data pitch, as is the case here. The results from four indentation depths were analyzed, which corresponded to compressive forces of 3.7N, 11.4N, 19.1N, and 26.8N respectively and the measured and predicted results are shown in figures 3 and 4.

It is inevitable that uncertainty is present in the measured data and that there is a further contribution from the decomposition process. These uncertainties are represented in figures 3 and 4 by a zone bounded by two parallel lines defined by

$$S_M = S_E \pm 2u(S_E) \tag{3}$$

where S_E and S_M are the sets of moments representing the displacements fields from the experiment and model respectively and $u(S_E)$ is the uncertainty present in the experimental data after decomposition and is the r.m.s. value of the minimum measurement uncertainty [14] and the decomposition uncertainty. The values of these uncertainties were found to be 28.76 μm and 8.11μm respectively using procedures described previously by Patterson et al., [14] and Tan et al., [9] respectively. For perfect agreement between measured and predicted results all of the data points in figures 3 and 4 would lie on the line, S_M=S_E, but agreement can be considered acceptable and the model valid when the data points lie within the zone described by equation (3) [16]. This occurs in Figure 3 at indentation depths between 0 mm and 2.2 mm for u and v displacements. In order to observe the trends more clearly, linear regression lines were fitted to each set of data and should have a gradient close to one when the model is valid. In this case, the theory is becoming a poor

representation when the depth of indentation reaches 3.3 mm because the regression line for the u displacement just falls outside of the uncertainty band at the extremes of the graph. The theory is not invalid at this depth of indentation because none of the data fall beyond the uncertainty zone. However, the theory can be considered invalid when the indentation depth increased to approximately 4.3 mm, since data points for both displacement fields lie outside the uncertainty band. Similarly, this analysis method was also applied to the rest of the wedges and the results are shown in figures 4.

3.2 Strain Fields

The strain field in the experiments can be derived from the spatial derivatives of the measured displacements. Rubber and rubber-like soft materials, which can experience very large elastic deformation before failure, are known as hyper-elastic materials. They experience large displacements and strains when subject to loading by a rigid wedge, and thus present a very complicated mechanical behaviour that cannot be modelled using linear elastic theory. Instead, it is more appropriate to use the finite deformation elasticity theory, in which the strain fields in a polar coordinate system are described by [18]:

$$\begin{aligned}
\varepsilon_r &= \frac{\partial u_r}{\partial r} + \frac{1}{2}\left[\left(\frac{\partial u_r}{\partial r}\right)^2 + \left(\frac{\partial u_\theta}{\partial r}\right)^2\right] \\
\varepsilon_\theta &= \frac{1}{r}\frac{\partial u_\theta}{\partial \theta} + \frac{u_r}{r} + \frac{1}{2}\left[\left(\frac{1}{r}\frac{\partial u_\theta}{\partial \theta} + \frac{u_r}{r}\right)^2 + \left(\frac{1}{r}\frac{\partial u_r}{\partial \theta} - \frac{u_\theta}{r}\right)^2\right] \\
2\varepsilon_{r\theta} &= \frac{\partial u_\theta}{\partial r} + \frac{1}{r}\frac{\partial u_r}{\partial \theta} - \frac{u_\theta}{r} + \frac{\partial u_r}{\partial r}\left(\frac{1}{r}\frac{\partial u_r}{\partial \theta} - \frac{u_\theta}{r}\right) + \frac{\partial u_\theta}{\partial r}\left(\frac{1}{r}\frac{\partial u_\theta}{\partial \theta} + \frac{u_r}{r}\right)
\end{aligned} \tag{4}$$

where (r, θ) are polar coordinates in the reference configuration as illustrated in Figure 1; u_r and u_θ are radial and circumferential displacements respectively. Since the experimental displacement field was obtained in a Cartesian coordinate system, it was necessary to use the following relationships to evaluate the partial derivatives of u_r and u_θ:

$$\begin{aligned}
\frac{\partial u_r}{\partial r} &= \left(\frac{\partial u}{\partial x}\cos\theta + \frac{\partial u}{\partial y}\sin\theta\right)\cos\theta + \left(\frac{\partial v}{\partial x}\cos\theta + \frac{\partial v}{\partial y}\sin\theta\right)\sin\theta \\
\frac{\partial u_r}{\partial \theta} &= \left(\frac{\partial u}{\partial y}x - \frac{\partial u}{\partial x}y\right)\cos\theta - u\sin\theta + \left(\frac{\partial v}{\partial y}x - \frac{\partial v}{\partial x}y\right)\sin\theta + v\cos\theta \\
\frac{\partial u_\theta}{\partial r} &= -\left(\frac{\partial u}{\partial x}\cos\theta + \frac{\partial u}{\partial y}\sin\theta\right)\sin\theta + \left(\frac{\partial v}{\partial x}\cos\theta + \frac{\partial v}{\partial y}\sin\theta\right)\cos\theta \\
\frac{\partial u_\theta}{\partial \theta} &= \left(\frac{\partial u}{\partial x}y - \frac{\partial u}{\partial y}x\right)\sin\theta - u\cos\theta + \left(\frac{\partial v}{\partial y}x - \frac{\partial v}{\partial x}y\right)\cos\theta - v\sin\theta
\end{aligned} \tag{5}$$

where (x, y) are the Cartesian coordinates shown in Figure 1; and u are v are horizontal and vertical displacements respectively. The experimental radial strain ε_r, circumferential strain ε_θ, and shear strain $\varepsilon_{r\theta}$ in the polar coordinate system can be obtained by substituting equation (4) into equation (3). Typical results are shown in Figure 5 for the 15° wedge with an applied indentation depth of 3.3mm (≡ 19.1N).

4. DISCUSSION

4.1 Displacement fields

The displacement data from the experiments and from the theory due to Ciavarella et al. [10] are compared for the 15°, 45°, and 73.5° wedges in Figure 4. For the 15° wedge, all of the data for u and v displacements lie within the uncertainty band for depths of indentation from 0mm to approximate 3.7 mm, which implies that the theory can be taken as confirmed for these levels of indentation but becomes invalid at some depth of indentation between 3.7mm and 4.7 mm since for an indentation of 4.7mm some of the data points lie outside the uncertainty band.

The regression line gradient progressively deviates from unity with increasing depth of indentation, implying the theory is an increasingly inaccurate representation of the experiment. For the 45° wedge, the theory is apparently less good than for 15° wedge since it becomes invalid at an indentation depth of greater than 2.8 mm but less than 4.54mm with the scatter of the data points increasing and a growing number lying outside the zone defined by equation (3). Not surprisingly, the theory breaks down even earlier for the 73.5° wedge with some data outside of the acceptable zone at an indentation depth of 3.2mm and the regression line gradient close to zero, signifying that the theory is no longer applicable to this specific case.

The tendency in Figures 3 and 4 is clear, i.e. the sharper the wedge, the smaller the indentation at which the theory fails. It should be mentioned that, although the geometry used in the experiments and for the theoretical solution was the same, the theory describes an idealized case that includes the following assumptions: the half-plane hypothesis is justifiable, zero interfacial friction, elastically similar contacting bodies, very small external wedge angle and sin $\theta \approx \theta$. Thus the results are not unexpected since more assumptions in the theory are contravened when the depth of indentation is greater. However, it is noteworthy that the theory breaks down at smaller values of indentation for the 5° than the 15° wedge. In order to find out a reasonable explanation for this, a theoretical solution for wedge-shaped blunt punch [19] was evaluated and compared using the same procedure. The interior stress distribution on the half plane can be expressed, using wedge-shaped blunt punch theory as

$$\begin{cases} \sigma_x = -\dfrac{4y\cot\theta}{A\pi^2}\displaystyle\int_{-a}^{a}\frac{arch(a/x)(x-s)^2}{[(x-s)^2+y^2]^2}d_s \\ \sigma_y = -\dfrac{4y^3\cot\theta}{A\pi^2}\displaystyle\int_{-a}^{a}\frac{arch(a/x)}{[(x-s)^2+y^2]^2}d_s \\ \tau_{xy} = -\dfrac{4y^2\cot\theta}{A\pi^2}\displaystyle\int_{-a}^{a}\frac{arch(a/x)(x-s)}{[(x-s)^2+y^2]^2}d_s \end{cases} \tag{6}$$

The displacement fields were found using the same method as mentioned in section 3.1 and subsequently decomposed as described above to yield moments which were compared to those obtained from experiments as shown in figure 6 for the 5° wedge. The solution remains valid for indentation depths from 0 mm to 3.3 mm but is not valid at an indentation depth of 4.3 mm, although only one point is outside of the uncertainty zone, which is an apparent improvement on the solution due to Ciavarella et al. [10].

It would appear that, with increasing indentation depth, there exists a critical value of indentation at which these theories are no longer applicable to this particular problem, probably because both are founded on linear elasticity. This critical value can been identified as when the regression lines in figures 3, 4 and 6 no longer fall in the zone defined by equation (3) for values of S_M and S_E in the range of the calculated moments, i.e. -100μm to 200μm, which gives rise to the concept of limiting gradients that fit within the uncertainty zone, as shown in figure 7 for the 5° wedge. Also shown in

figure 7 are the regression line gradients for the horizontal and vertical displacements obtained from the graphs in figure 3 as a function of the critical value of applied load. Similar plots were produced for each wedge angle examined and the critical values are shown in Figure 8 on the load-indentation curves for each experiment. The critical value for the theory due to Ciavarella et al. [10] increases linearly from an indentation depth of about 1.5mm for the 75° wedge through about 2.75mm for the 45° wedge to about 4.3 mm for the 15° wedge, and then drops to about 3.1 mm for the 5° wedge. The critical indentation depth for blunt punch theory applied to the 5° wedge is also shown.

Ciavarella et al. [10] assumed that the blunt wedge had a rounded tip, whereas the curvature at the wedge tip is ignored in the blunt punch theory. The difference in geometry caused a difference in the predicted distribution of contact pressure which in turn affected the displacement field. In the experiment, all of the indenters were manufactured with the same tip radius, R=1.68mm and therefore the half-width of the tip becomes smaller as the angle of the wedge decreases. In this case, the half-width of the tip is 0.145mm for the 5° wedge, which is negligible when compared to the contact width at higher indentation depths, which probably accounts for the better fit of blunt punch theory than Ciavarella's solution to the measured data.

4.2 Strain fields

Although Gao and his co-workers [6 - 8] divided the strain field created in a rubber block into expanding (EX) and shrinking (SH) sectors for which the strain fields can be found separately, there has been no experimental verification of this 'sector division methodology'. The circumferential strain field observed in Figure 5 appears to be composed of two axially symmetry sectors, i.e. an expanding (EX) sector directly below the contact and a shrinking (SH) sector on either side of the contact. The transition between these sectors can be taken as the null or zero-valued contours of the circumferential (or radial) strain. These boundaries for five loading steps are plotted in Figure 9 for each indenter. The 'opening' angle between the boundaries was estimated using a regression line fitted to each boundary and included as a label in the figure. By comparing the plots in Figure 9, it is obvious that the expanding sector becomes larger when the wedge-shaped indenter is sharper and conversely the expanding sector becomes smaller and narrower with increasing load. For example, the 'opening' angle gradually decreases from 159 degree to 100 degrees for the 5° wedge as the applied load

increases from 3.7N to 34.5N. These trends are summarised in figure 10 where the 'opening angle' of the boundary between the expanding (EX) and shrinking (SH) sectors is plotted as a function of applied load for each wedge angle. The trends appear to be asymptotic with load implying that the shape of the sectors will stabilise at high loads and remain constant until failure in the material of the block.

It is interesting to observe that EX, the expanding sector becomes smaller with increasing load and it is difficult to interpret this trend with any certainty. However, it is reasonable to speculate that when the wedge angle is very shallow, i.e. 5 to 15 degrees, then we can consider a small element *A* located in the EX sector and close to both the contact surface and the initial boundary of EX and SH, as illustrated in the upper sketch of Figure 11. For small depths of indentation, element *A* is mainly subject to compression in the radial direction since the local stress field is dominated by the vertical compression from the indenter. As a result of Poisson ratio effects, the material in element *A* expands in the circumferential direction. For small wedge angles, the contact length increases faster with load leading to a more rapid change in the position of the sector boundaries. In addition, a longer contact length leads to more constraint along the contact interface which restricts expansion closer to the indenter, i.e. with increasing load, there is more constraint applied to element *A* in the circumferential direction. The components of stress in the two directions achieve a balance state when the load is moderate, that is, the deformation of element A is paused in this stage. After a short duration of equilibrium, compressive stress in the circumferential direction becomes larger than in radial direction due to the indentation of wedge and the corresponding rotation of material near contacting edge. Thus, the element *A,* which initially was located in the EX sector, is transformed into the SH sector in this last stage. This seems to provide a reasonable hypothetical mechanism for the change in size of the EX sector.

It should be noted that Gao and his co-workers obtained asymptotic solutions for the strain fields associated with contact of a rigid wedge with a rubber notch assuming two-dimensional plane strain deformation and therefore these solutions are not directly applicable to the case examined here where the rubber block is a plain rectangle initially and there is considerable out-of-plane deformation which invalidates the plane strain assumption.

5. CONCLUSIONS

Stereoscopic digital image correlation has been employed to measure the displacements resulting from indentation of a soft material block by a series of wedges with a round tip and various angles of slope. Experiments were performed with wedge angles that varied from sharp to blunt (73.5°, 45°, 15°, and 5°). The limits of validity for soft materials of the theory due to Ciavarella et al. (1998) were investigated by comparing measured and predicted in-plane displacement fields using image decomposition and found to be restricted to small indentation depths and small wedge angles. The classical blunt punch theory was also used for the smallest wedge angle and the results compared to both the predictions using the theory due to Ciavarella et al. and the results from the experiments. It has been found that both theories have a critical depth of indentation beyond which they are not valid probably as a result of non-linear behaviour in the experiment and this value can be evaluated quantitatively using the experimental analysis described above. The sectorial approach to modelling indented soft materials proposed by Gao and his co-workers has been verified by experiment and the evolution of sectors during indentation process is revealed for the first time.

ACKNOWLEDGEMENTS

Support from the National Basic Research Program of China (No, 2012CB937500) and National Natural Science Foundation of China (No. 11127292) is gratefully acknowledged. XT was a recipient of a China Scholarship Council Award (No 2011625016) and EAP was a recipient of a Royal Society Wolfson Research Merit Award. The support of the University of Liverpool in providing the laboratory facilities used in this investigation is gratefully acknowledged.

REFERENCES

1. Boussinesq J. *Applications des potentiels à l'etude de l'equilibre et du mouvement des solides elastiques.* Gauthier-Villars, Paris (1885).

2. Sneddon, I.N. The Relation between Load and Penetration in the Axisymmetric Boussinesq Problem for a Punch of Arbitrary Profile. *Int. J. Eng. Sci*. **3**, 47–57, (1965).

3. Hirst, W. and Howse M.G.J.W. The Indentation of Materials by Wedges. *Proc. R. Soc. Lond. A.* **311**, 429-444 (1969).

4. Sundaram, N., Guo, Y. and Chandrasekar, S. Modes of deformation and weak boundary conditions in wedge indentation. *Mrs Commun*., **2**, 47-50 (2012).

5. Korsunsky, A.M. The influence of punch blunting on the elastic indentation response. *J. Strain Anal. Eng. Des.,* **36**, 391-400 (2001).

6. Gao Y.C. and Gao, T.J. Large deformation contact of a rubber notch with a rigid wedge. *Int. J. Solids Struct.,* **37**, 4319-4334 (2000).

7. Chen, S.H. and Gao Y.C. Asymptotic analysis and finite element calculation of a rubber notch contacting with a rigid wedge. *Acta Mech.,* **147**, 111-124 (2001).

8. Gao Y.C. and Qian H.S. Analysis of the contact of a rubber notch with a rigid wedge. *Mech. Res. Commun.,* **29**, 165-176 (2002).

9. Tan, X.H., Kang, Y.L. and Patterson, E.A. An experimental study of the contact of a rounded rigid indenter with a soft material block. *J. Strain Anal. Eng. Des*., **49**, 112-121 (2014).

10. Ciavarella, M., Hills D. A. and Monno, G. Contact problems for a wedge with rounded apex. *Int. J. of Mech. Sci.,* **40**, 977-988 (1998).

11. Han Y.G., Rogalsky A.D., Zhao B. and Kwon H.J. The Application of Digital Image Techniques to Determine the Large Stress-Strain Behaviors of Soft Materials. *Polym Eng Sci*., **52**, 826-834 (2012).

12. Zhang Z.F., Kang Y.L., Wang H.W., Qin Q.H., Qiu Y. and Li X.Q. A novel coarse-fine search scheme for digital image correlation method. *Measurement*, **39**, 710-718 (2006).

13. Sutton, M. A., Orteu, J. J., and Schreier, H. *Image correlation for shape, motion and deformation measurements*. Springer, New York (2009).

14. Patterson, E.A., Hack, E., Brailly, P., Burguete, R.L., Saleem, Q., Seibert, T., Tomlinson, R.A. and Whelan, M. Calibration and evaluation of optical systems for full-field strain measurement. *Opt. Laser. Eng.,* **45**, 550-564 (2007).

15. Hills, D. A., Nowell, D. and Sackfield, A., *Mechanics of Elastic Contacts*. Butterworth-Heinemann, Oxford (1993).

16. Sebastian C., Hack E. and Patterson E.A. An approach to the validation of computational solid mechanics models for strain analysis. *J. Strain Anal. Eng. Des*., **48**, 36-47 (2013).

17. Sebastian, C.M., Patterson, E.A. and Ostberg, D. Comparison of numerical and experimental strain measurements of a composite panel using image decomposition. *App. Mech. Mat.,* **70**, 63-68 (2011).

18. Xiao X., Kang Y.L., Hou Z.D., Qiu W., Li X.L. and Li X.Q. Displacement and strain measurement by circular and radial gratings moiré method. *Exp. Mech*., **50**, 239-244 (2010).

19. Johnson K.L. *Contact mechanics*. Cambridge University Press, Cambridge (1985).

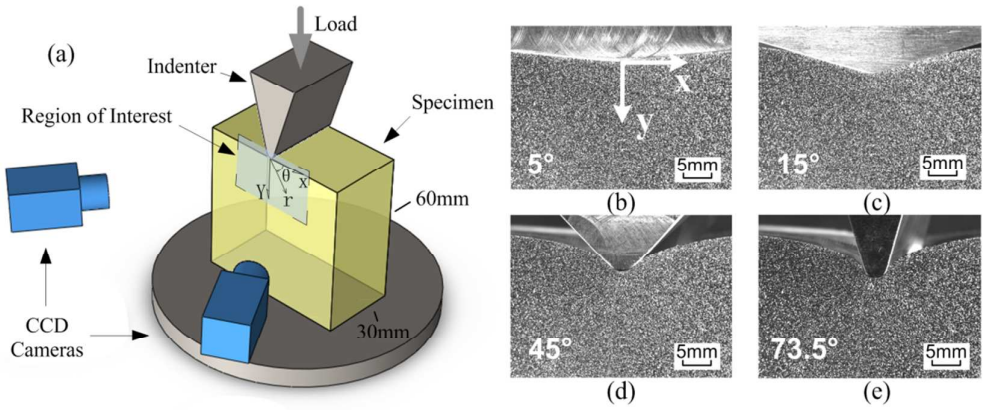

Figure 1 - Schematic arrangement of the experiment (*left*) with photographs of the four wedges each with a tip radius of 1.68mm indenting the rubber blocks (*right*).

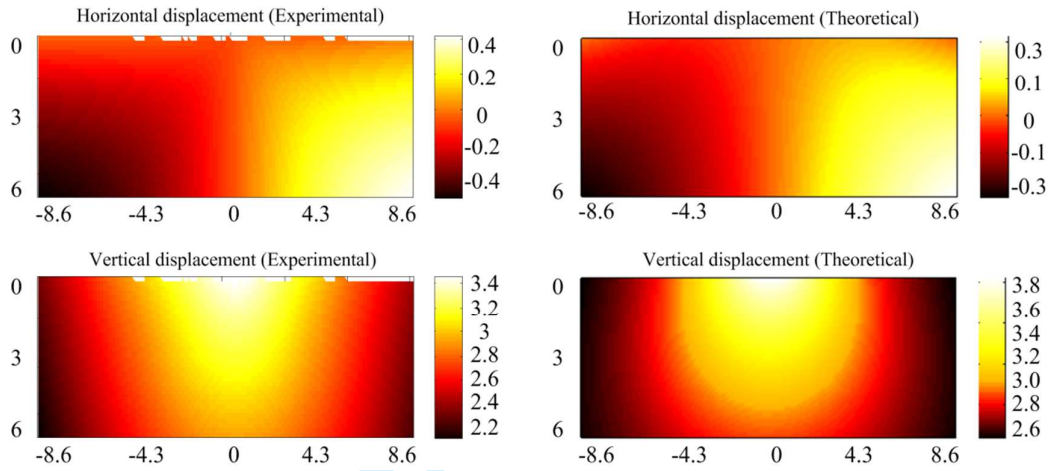

Figure 2 - Measured (left) and predicted (right) displacement fields for the area (6x17.2mm) in the rubber block immediately below the 15° wedge, which has been subjected to a nominal displacement load of 3.3mm (≡ 19.1 N) corresponding to tip-radius to depth of indentation ratio of 0.51. The tip of the wedge made contact with the block at x=0, y=0. Both the spatial units and units on the colour bars are millimetres.

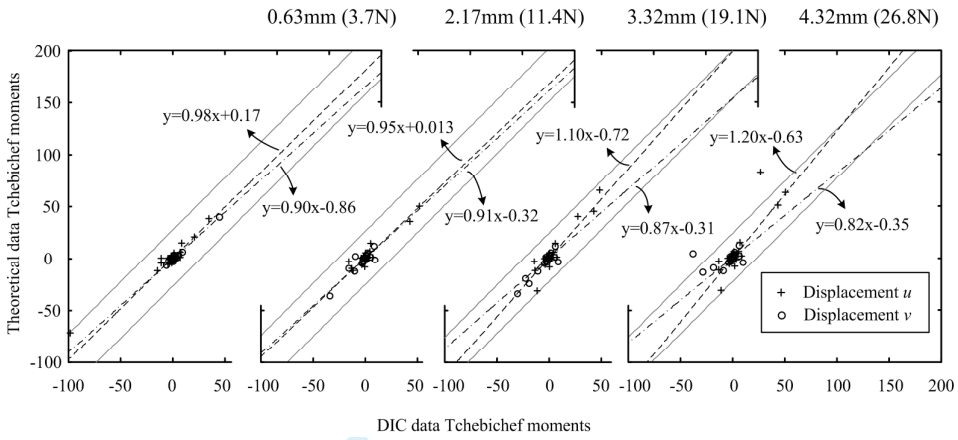

Figure 3 - Tchebichef moments describing the displacement fields from the solution due to Ciavarella et al. [10] compared to those from the experiment with a 5° wedge, with regression lines for u and v displacements (dash-dotted and long-dashed lines respectively) and the zone of measurement uncertainty defined equation (3) (solid grey lines). The tip-radius to indentation depths are 2.67, 0.77, 0.51 and 0.39 respectively from left to right.

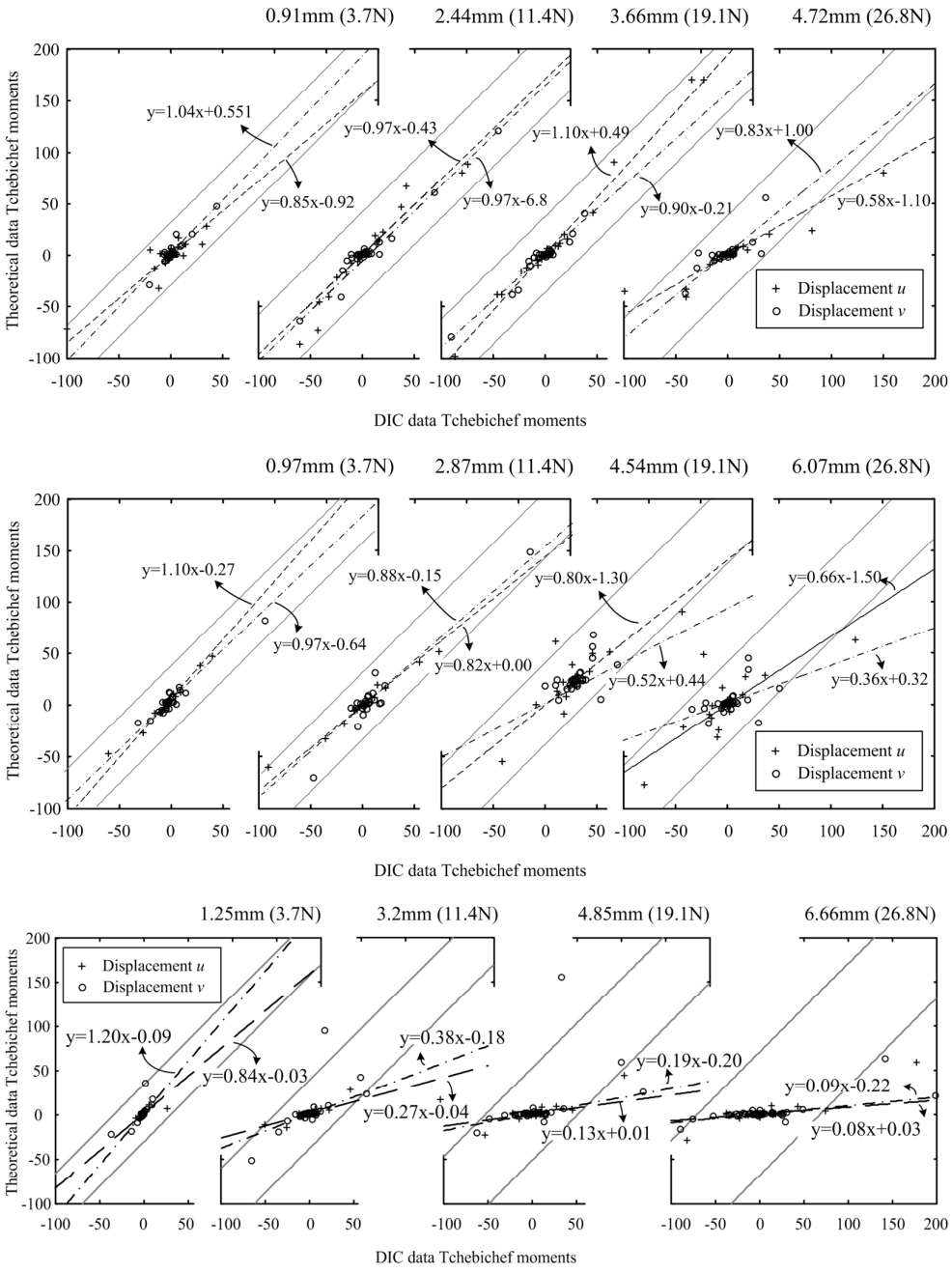

Figure 4 - Tchebichef moments describing the displacement fields from the solution due to Ciavarella et al. [10] compared to those from the experiment with the 15° (*top*), 45° (*middle*) and 73.5° (*bottom*) wedges, with regression lines for u and v displacements (dash-dotted and long-dashed lines respectively) and the zone of measurement uncertainty defined equation (3) (solid grey lines).

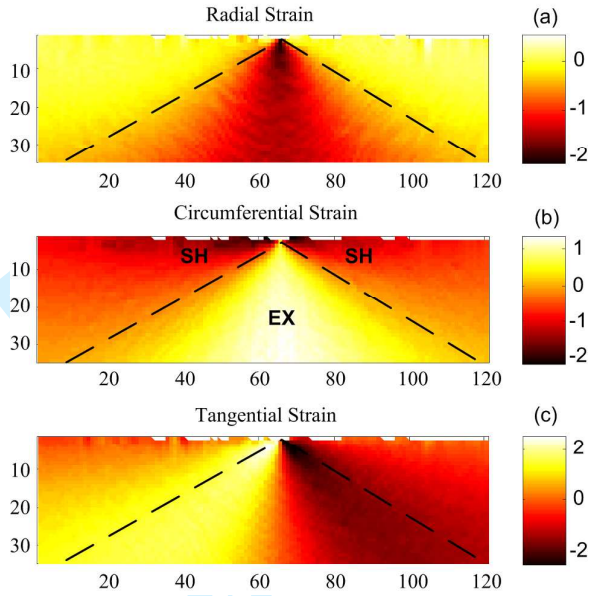

Figure 5 - Typical strain fields obtained from the measured displacements shown in figure 2 using finite deformation theory [equations (4) & (5)] with dashed lines superimposed to indicate the boundaries of the expansion (EX) and shrinkage (SH) sectors proposed by Gao & Gao [6].

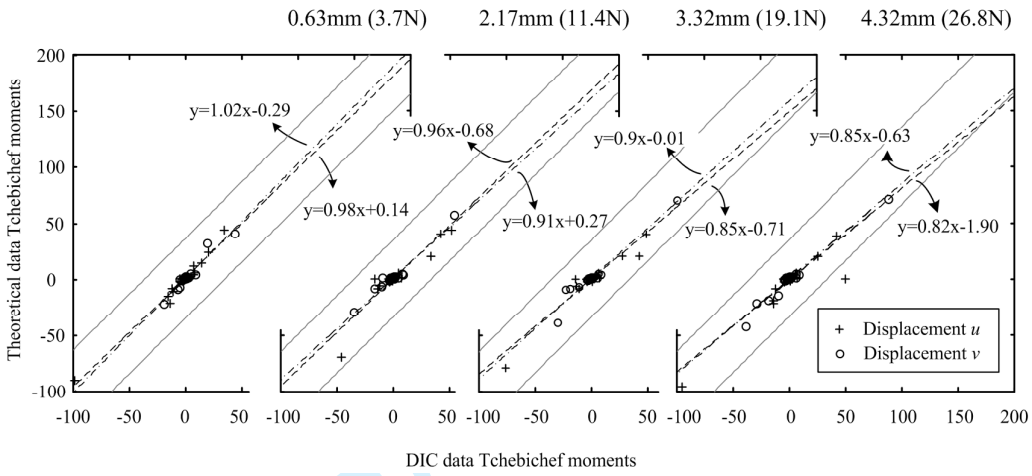

Figure 6 - Tchebichef moments describing the displacement fields from the blunt punch theory [19] compared to those from the experiment with the 5° wedge, with regression lines for u and v displacements (dash-dotted and long-dashed lines respectively) and the zone of measurement uncertainty defined equation (3) (solid grey lines).

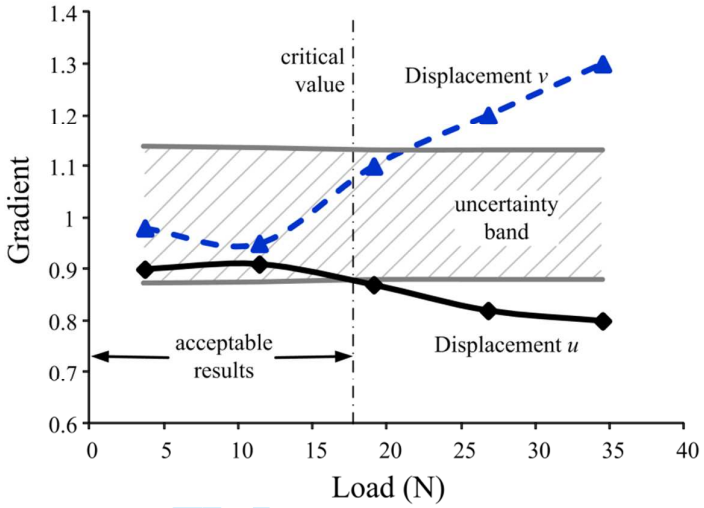

Figure 7 - Regression line gradients in Figure 3 as functions of the applied load; the shaded area is defined by the limiting gradients that remain within the uncertainty zones defined in Figure 3 by equation (3).

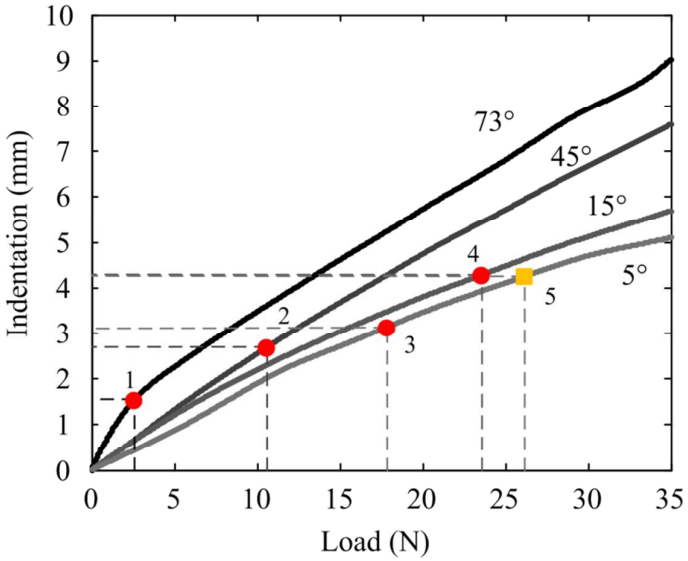

Figure 8 - Indentation-load curves for the rubber block indented by the four rigid wedges with different face angles together with the critical value (round symbols) at which the theory due to Ciavarella et al. [10] ceases to be valid based on graphs of the form shown in figure 7 plus the limit of validity of the blunt punch theory [19] for the 5 degree wedge (square symbol).

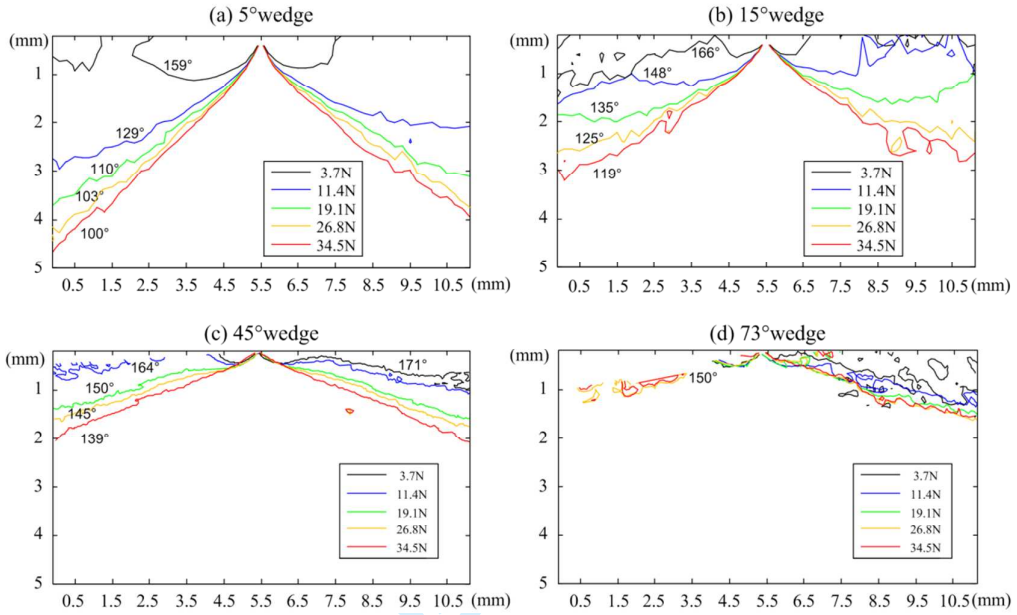

Figure 9 - The boundaries between the expanding (EX) and shrinking (SH) sectors defined by Gao & Gao [6] as a function of applied load for wedge angles of 5, 15, 45 and 73.5 degrees obtained from the measured deformation fields; the labels indicate the 'opening angle' of the boundaries.

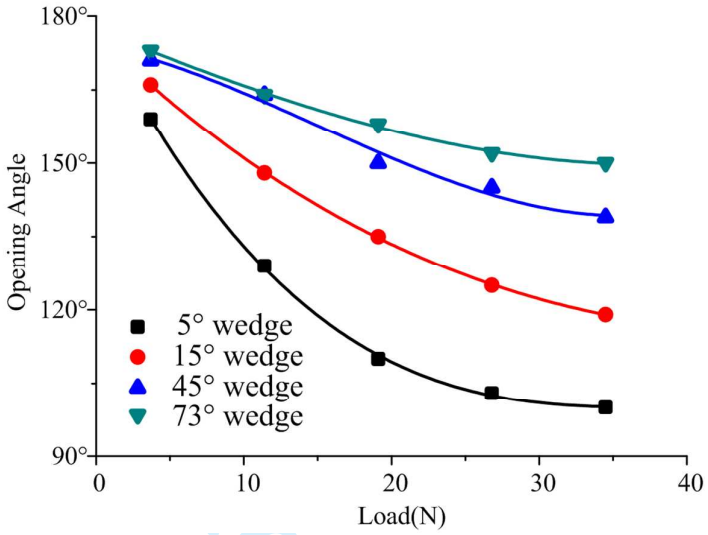

Figure 10 - The 'opening angle' of the sector boundaries in figure 9 plotted as a function of applied load.

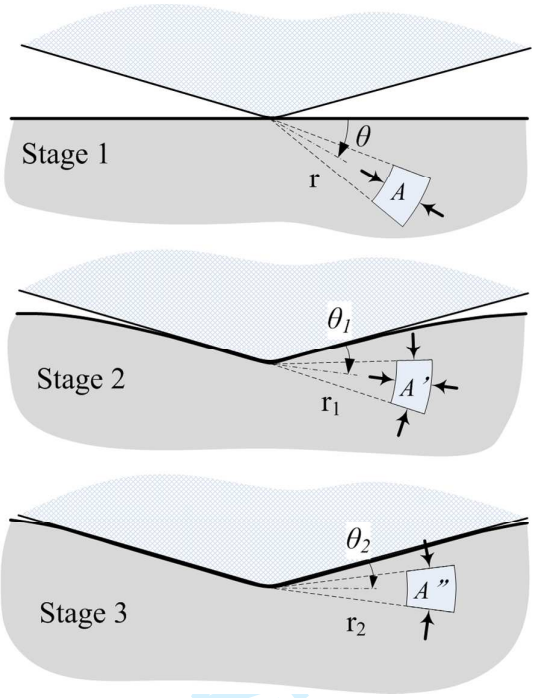

Figure 11 - Schematic diagram showing the progressive deformation of the rubber block by the wedge.